NANOSYSTEMS:
PHYSICS, CHEMISTRY, MATHEMATICS

Original article

Muhammad Irfan Asghar, et al. *Nanosystems: Phys. Chem. Math.*, 2022, **13** (2), 181–191.
http://nanojournal.ifmo.ru
DOI 10.17586/2220-8054-2022-13-2-181-191

Synthesis, characterization and electrical properties of the nanosized perovskite $LaFeO_3$

Muhammad Irfan Asghar[1,a], Muhammad Kashif Shahid[2,b], Muhammad Haq Nawaz[3,c], Muhammad Idrees[1,d], Muhammad Asif[4,e], Ahsan Ali[5,f]

[1]Department of Physics, COMSATS University Islamabad, Lahore Campus, Pakistan

[2]Research Institute of Environment & Biosystem, Chungnam National University, Daejeon, Republic of Korea

[3]Department of Physics, University of Gujrat, Hafiz Hayat Campus, Gujrat, Pakistan

[4]Department of Physics, University of Engineering and Technology Lahore, Pakistan

[5]School of Mechanical Engineering, University of Leeds, Leeds LS2 9JT, UK

[a]irfanmeo1@gmail.com, [b]mkbutt2000@gmail.com, [c]haqn5656@gmail.com,
[d]midrees@cuilahore.edu.pk, [e]asif81292@yahoo.com, [f]ahsanali23654@gmail.com

Corresponding author: Muhammad Idrees, midrees@cuilahore.edu.pk

ABSTRACT Single-phase highly crystalline $LaFeO_3$ is synthesized by autocombustion of the gel complex obtained from citrate and metal nitrate precursors. The XRD analysis exhibited the transformation of amorphous phases of La_2O_3 and Fe_2O_3 into highly crystalline $LaFeO_3$ at 1000 °C. The agglomerated semi spherical morphology is observed. The average particle size of sintered pellets at 1000 °C for 4 h, 8, 12, and 16 h heating time is found 105, 130, 160 and 200 nm, respectively. TGA analysis revealed 27% weight lost due to the decomposition of $La(OH)_3$ and $Fe(OH)_3$ into La_2O_3, Fe_2O_3, and $LaFeO_3$. Electrical properties of $LaFeO_3$ were found to be dependent on micro-structural heterogeneities i.e., grain and grain boundaries. Two probe DC resistivity exhibited decrease in resistance with increasing heat treatment and time. The outcomes of this study confirmed the potential applications of perovskite-type $LaFeO_3$ in energy and environmental sectors.

KEYWORDS Impedance spectroscopy, $LaFeO_3$, perovskite, sintering, TGA

ACKNOWLEDGEMENTS Authors thank to the National Centre for Physics, Islamabad for assistance in instrumental analysis.

FOR CITATION Muhammad Irfan Asghar, Muhammad Kashif Shahid, Muhammad Haq Nawaz, Muhammad Idrees, Muhammad Asif, Ahsan Ali Synthesis, characterization and electrical properties of the nanosized perovskite $LaFeO_3$. *Nanosystems: Phys. Chem. Math.*, 2022, **13** (2), 181–191.

1. Introduction

While industrial development has improved the quality of life with the remarkable inventions and revolutions, it has also created several issues and challenges related to the environment and energy [1]. The need for solutions to environmental issues and alternative energy sources has increased the interest in synthesis and application of new materials [2–4]. In recent years, much attention is given to the perovskite materials for their substantial optical and electrical characteristics [5,6]. Recently, novel materials having perovskite structures, including $HoFeO_3$ [7], $GdFeO_3$ [8] $CaMnO_3$ [9] $Nd_{1-x}Sr_xFeO_3$ [10], $YbFeO_3$ [11] $SmFeO_3$ [12] etc. have been thoroughly studied Lanthanum orthoferrite ($LaFeO_3$), is one of the recognized perovskite-type oxides. It has an orthorhombic perovskite structure with space group Pbnm [13] $LaFeO_3$ constitutes FeO_6 units with La^{3+} ions inserted between these units [14]. Considering Neel temperature (T_N) of 740 K bulk $LaFeO_3$ is known to be antiferromagnetic [15]. The prominent mixed conductivity properties of $LaFeO_3$ encourage its electro-ceramic applications. It is chemically stable in both reducing and oxidizing environments With atomic doping of $LaFeO_3$, several improved properties can be achieved including higher electrical conductivity, greater dielectric constant and low dielectric loss susceptibility, polarizability and average type of permittivity [16, 17] Several methods have been introduced for the synthesis of $LaFeO_3$ [18]. These methods include the thermal decomposition of the coprecipitated precursor [$La(OH)_3$ and $Fe(OH)_3$], calcination of a mixture of La_2O_3 and Fe_2O_3, and the thermal decomposition of heteronuclear complex i.e., $La[Fe(CN)_6$ [19] $LaFeO_3$ is found to be synthesized at 600, 800 and 1000 °C from La-Fe-(CN), La-Fe-OH and La-Fe-O respectively. The uniform atomic level structure of $LaFeO_3$ is obtained during thermal decomposition of the $La[Fe(CN)_6]\cdot 5H_2O$ heteronuclear complex. Hence, the low temperature condition favored the synthesis of pure $LaFeO_3$ nanoparticles.

Another study used $La_2(CO_3)_3$ and $Fe(CO)_5$ as a starting material for the synthesis of nanocrystalline perovskite-type $LaFeO_3$ via sonochemical method [20]. The highly crystalline and homogenized product is obtained and the particles were found to have 30 nm size, as confirmed by transmission electron microscopy (TEM). The coercivity and saturation magnetization of the particles were found 250 H_c and 40 memu g^{-1}, respectively. The shorter annealing time and lower

processing temperature increase the significance of this method than that of other chemical techniques that involve the longer soaking and very high calcination temperature. It is noteworthy that longer soaking and higher temperature result in high porosity and poor uniformity that may affect the properties of the powder [20].

A study reported the synthesis of nanosized (30 nm) $LaFeO_3$ powder via sol-gel auto-combustion method [21]. The process involved the homogeneous sol formation followed by dried gel formation and combustion of dried gel. The citrate-based sol-gel pathway is also introduced for the synthesis of uniform $LaFeO_3$ nanowires [22]. Other methods for synthesis of $LaFeO_3$ include glycine combustion method [23], SBA-16 template method [24], microwave-assisted method [25], glucose sol-gel method [26], solid-state reaction method [27], starch assisted soft-chemistry method [28], high energy milling [29], floating zone method [30], and auto-combustion of the gel complex acquired from metal nitrate and citrate precursor [31].

The main objective of this study is to synthesize the single-phase highly crystalline perovskite-like $LaFeO_3$ for practical application in the field of energy and environment. The influence of sintering conditions on the phase transformation is determined via advanced characterization techniques and the results are discussed concisely. The electrical properties of perovskite-like $LaFeO_3$ are also determined. Based on findings of this study, perovskite-like $LaFeO_3$ is proposed for practical application in the field.

2. Materials and methods

2.1. Chemicals and reagents

All the chemicals and reagents used in this study were of analytical grade and used as received. Lanthanum nitrate hexahydrate and iron nitrate nonahydrate were purchased from Sigma-Aldrich.

2.2. Synthesis of $LaFeO_3$

The appropriate amount of lanthanum nitrate hexahydrate [$La(NO_3)_3{\cdot}6H_2O$], citric acid monohydrate [$C_6H_8O_7{\cdot}H_2O$] and iron (III) nitrate nonahydrate [$Fe(NO_3)_3{\cdot}9H_20$] were dissolved (separately) in deionized water to achieve 0.1 M concentration (Fig. 1). Both nitrate solutions were mixed in glass beaker and stirred for 45 min. The prepared solution was dropwise added into the 500 mL solution of citric acid monohydrate. The mixture was heated to 70–75 °C. Followed by evaporation of solvent, wet yellow gel is obtained that was further dried in electric furnace (100 °C). The dried gel is ground and kept in the glass beaker. The top of beaker is covered with aluminum foil and small holes were made in the foil. The beaker was placed in furnace and the temperature is increased to 150 °C with the increasing rate of 5 °C/min. The brown color precipitate is collected at bottom that was ground to the fine particles. The obtained particles were sintered at different temperatures (450, 600, 800 and 100 °C) for 4 h. The obtained products were named as described in Table 1.

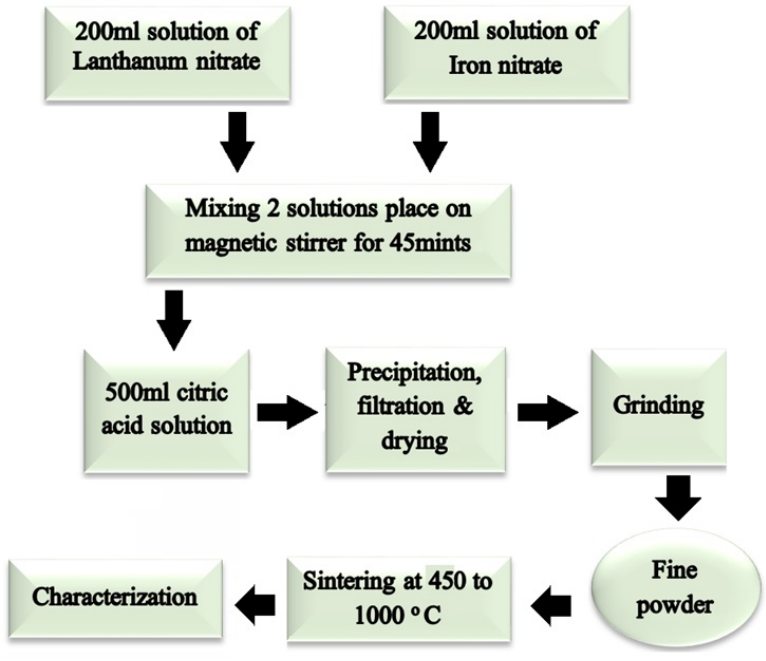

FIG. 1. Scheme of $LaFeO_3$ synthesis

TABLE 1. List of samples prepared with different sintering conditions

Sample identity	Sintering conditions
LFO-COP-Precipitates	precipitated powder
LFO-COP-450 °C	sample treated at 450 °C for 4 h
LFO-COP-600 °C	sample treated at 600 °C for 4 h
LFO-COP-800 °C	sample treated at 800 °C for 4 h
LFO-COP-1000 °C	sample treated at 1000 °C for 4 h

2.3. Instrumentation

Different characterization techniques are applied to identify the elemental and morphological properties of the synthesized products. Temperature of electric furnaces is internally controlled. The crystallization progression was examined by differential thermal analysis (DTA) and thermogravimetric analysis (TGA). The surface morphology and crystalline structure of $LaFeO_3$ is examined by scanning electron microscope (SEM) and X-ray diffraction (XRD), respectively. The resistance and capacitance characteristics of $LaFeO_3$ are measured via impedance spectroscopy.

3. Results and discussion

3.1. Thermal analysis

Fig. 2 shows the thermal decomposition progression of $LaFeO_3$. A small endothermic peak was appeared at 330 °C and the sharp change in phase is started after 600 °C The weight loss is proceeded up to 800 °C in several steps. About 27% weight loss is observed due to the decomposition of $La(OH)_3$ and $Fe(OH)_3$ present in the total mass of the sample. The decomposition of hydroxides resulted in the La_2O_3, Fe_2O_3 and $LaFeO_3$ phases. This weight loss was found in consistent with reported value of 27.5% [20]. About 90% decomposition of hydroxides is achieved at 650 °C. A negligible weight loss is observed when the temperature is increased from 800 to 1200 °C. The heat absorption at 800 °C is intensely reduced when compared to 600 °C, however, a minor heat absorption was observed up to 1200 °C. Although LFO450 and LFO600 contributed to initiate the transformation of amorphous phases, these conditions are not enough to achieve the higher crystaline form of $LaFeO_3$. The single crystalline phase of $LaFeO_3$ is started at 800 °C. The slight loss in weight from 800 to 1200 °C is attributed to the loss of minute quantity of oxygen [32].

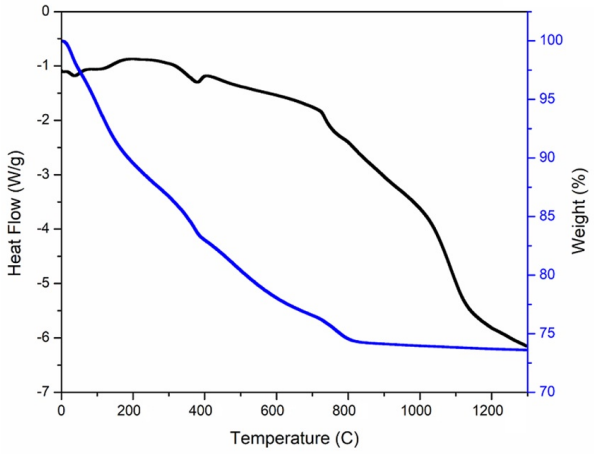

FIG. 2. TGA results of the precipitated powder

3.2. XRD analysis

The XRD analysis of the precipitate and the sintered samples is conducted to determine the phase transformation and crystallinity of the material. Fig. 3 shows the XRD pattern of the precipitate. The diffraction peaks observed at the 2θ of 27.5°, 28.1°, 39.8°, 48.8°, 55.7° and 64.8° represented the crystalline planes of $La(OH)_3$ (110), (101), (201), (211), (112) and (311), respectively. The corresponding planes were compared with the standard XRD pattern of $La(OH)_3$ (JCPDS card No. 36-1481) and found in fine agreement with earlier studies [33, 34]. In addition, the diffraction peaks at the 2θ of 22.1°, 26.0°, 38.5°, 42.6°, 43.9°, 61.4° and 70.0° indicated a phase of $Fe(OH)_3$ The major peaks of amorphous

phase of $Fe(OH)_3$ found at 2θ of 38.5°, 42.6° and 43.9° assigned to the corresponding (031), (222) and (213) planes, respectively [35] The characteristic peaks of $Fe(OH)_3$ were also found in good agreement with standard pattern (JCPDS card 38-0032).

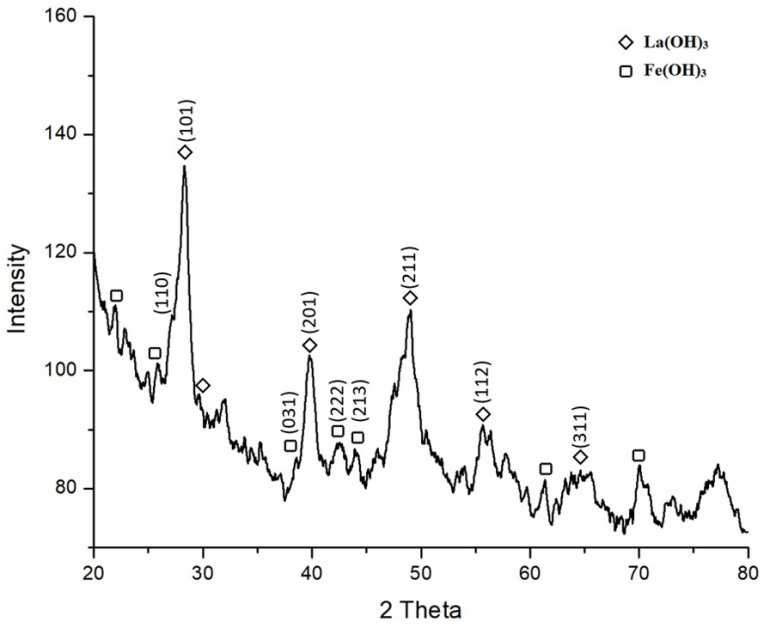

FIG. 3. XRD pattern of LFO-COP-Precipitate

Followed by 4 h sintering at 450 °C, a peak appeared at 2θ of 31.6° indicated the presence of $LaFeO_3$ due to the onset of the reaction between $Fe(OH)_3$ and $La(OH)_3$ (Fig. 4). However, the existence of $LaFeO_3$ is not highly marked due to the incomplete transformation of $La(OH)_3$ and $Fe(OH)_3$ in to $LaFeO_3$. Another study found that the diffraction peaks of $LaFeO_3$ remains uncertain when the sample is calcined below 500 °C [24]. The major reason behind this phenomenon is the low crystallinity and higher amorphous phase of $LaFeO_3$. In addition, differential peaks corresponding to Fe_2O_3 and La_2O_3 were also found, as compared with the reported spectra of Fe_2O_3 [36] and La_2O_3 [37]. It is noteworthy that the amorphous phases of hydroxides started transformation into crystalline form due to heat treatment.

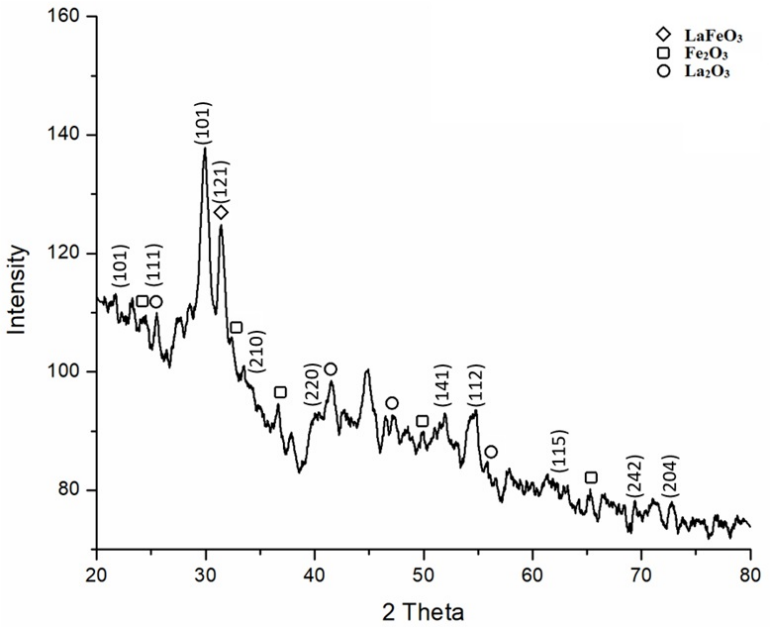

FIG. 4. XRD pattern of LFO-COP-450 °C

The samples obtained after 4 h sintering at 600 °C also displayed the amorphous phase of $LaFeO_3$, Fe_2O_3 and La_2O_3 as shown in Fig. 5. XRD pattern of LFO 600 revealed the higher crystallinity than that of LFO 450. This is found in

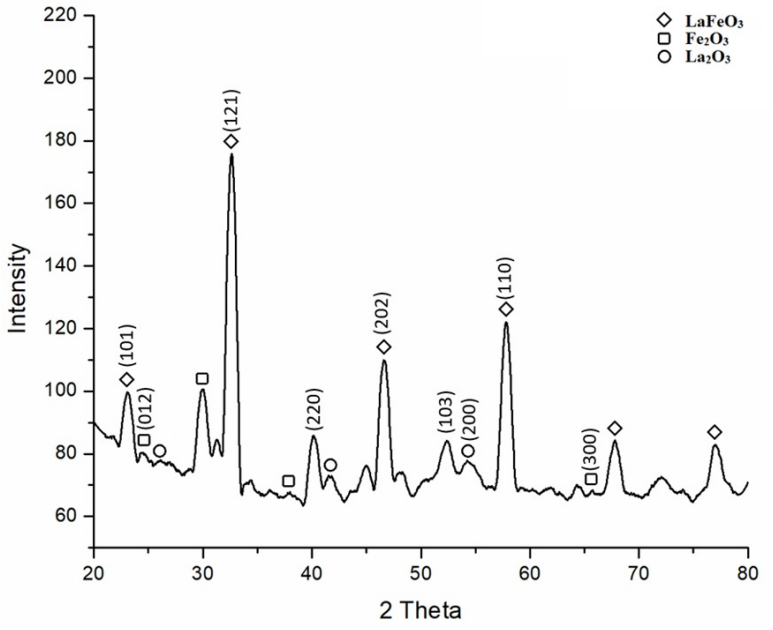

FIG. 5. XRD pattern of LFO-COP-600 °C

consistence with TGA results, where, 90% of hydroxides were decomposed when 600 °C is applied. Fig. 6 shows the XRD pattern of particles sintered for 4 h at 800 °C. The diffraction peaks observed at the 2θ of 231°, 32.5°, 40.1°, 46.8°, 57.9°, 67.0° and 77.5° represented the crystalline planes of $LaFeO_3$ (101), (121), (22), (202), (123), (004) and (204), respectively. The obtained data was appeared in fine agreement with a reported XRD pattern of $LaFeO_3$ that is calcined at 850 °C [38]. Although the higher level of crystallization is evident from the XRD pattern of LFO 800, some impurities such as La_2O_3 and Fe_2O_3 are also observed.

Although, the XRD pattern of the as-burnt powder is attributable to a mixture of amorphous and crystalline phases, heat treatment progressively improved the crystallinity of the powder to a well crystalline phase at 800 °C. All the XRD peaks are well indexed by an orthorhombic unit cell of $LaFeO_3$ with space group of Pbnm (JCPDS 37-1493). Substantial variations in the peak intensity and full width at half maximum (FWHM) of orthoferrite peak were identified during heat treatment. It is found that FWHM of the orthoferrite peak decreased as we increased the temperature of heat treatment. This infers an increase in crystallite size at higher temperatures. The average crystallite sizes determined by Scherer's formula were 12, 23 and 43 nm for LFO450, LFO600 and LFO800, respectively. $LaFeO_3$ phase formation during ignition and increase in crystallinity with increase in heat treatment temperature were appeared in fine agreement with the reported studies [39].

Further sintering at 1000 °C resulted in the formation of the crystalline phase of $LaFeO_3$, as identified via XRD analysis (Fig. 7). All the diffraction peaks were attributed to the single crystalline phase of $LaFeO_3$ without any impurity. The obtained pattern was found in consistence with the standard pattern of orthorhombic $LaFeO_3$ (JCPDS card 37-1493). The calculated cell parameters of $LaFeO_3$ were $a = 5.563$, $b = 5.562$ and $c = 7.868$. The diffraction peaks and corresponding crystalline planes were also found in fine agreement with earlier studies [16, 40]. The effect of sintering time on the crystalline structure of synthesized $LaFeO_3$ is also assessed. $LaFeO_3$ pellets were prepared under 40 bar hydraulic pressure and sintered at 1000 °C by keeping in a ceramic boat for 4, 8, 12 and 16 h. The XRD pattern of all the samples is presented in Fig. 8. All the spectra indicated the single crystalline phase of $LaFeO_3$. However, an increase in the time of heat treatment resulted a slight shift in diffraction peaks towards higher or lower angle from their actual position. This phenomenon indicates the compressive strain and decrease in the length of the cell parameters. As shown in Fig. 8, at 4 h we can see that there is a non uniform strain in which broading of the peak is visible whereas, the peak position is shifted toward the higher angle due to the uniform strain in case of 8 h sample. The XRD pattern after 12 h did not indicate any strain and peak was found at its original position. In case of 16 h treatment, the peak is again shifted to the higher angle from their original position that is an indication of uniform strain.

3.3. SEM Analysis

Fig. 9 shows the SEM images of the $LaFeO_3$ sintered at different conditions. The microstructure shows that particles have sharp grain boundaries and well defined geometric shapes. The agglomerated semi spherical particles were found similar to the reported nano scale structure of $LaFeO_3$ [41]. A prominent difference is observed in size of the particles sintered for the different time duration. It is found that the particle size is expanded with increasing the duration of heat treatment. Another study also found the similar expansion in particle size, when the $LaFeO_3$ is sintered at higher

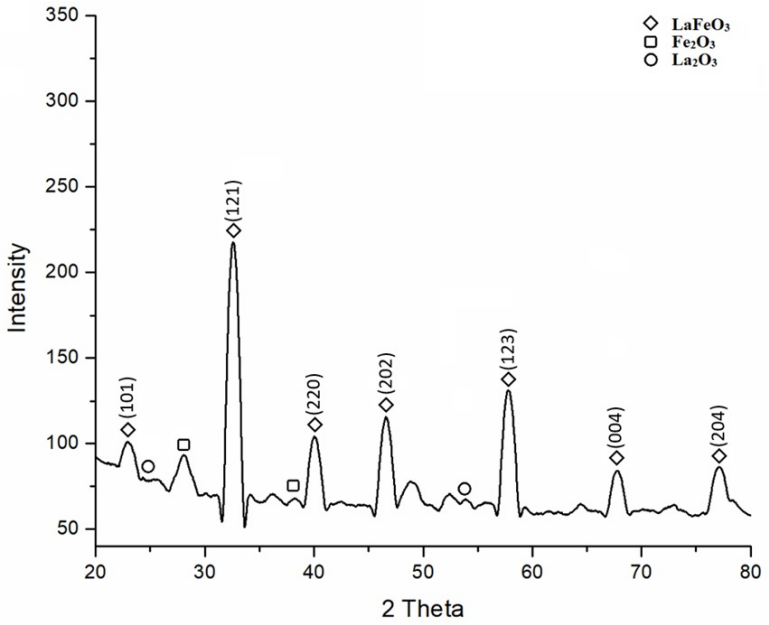

FIG. 6. XRD pattern of LFO-COP-800 °C

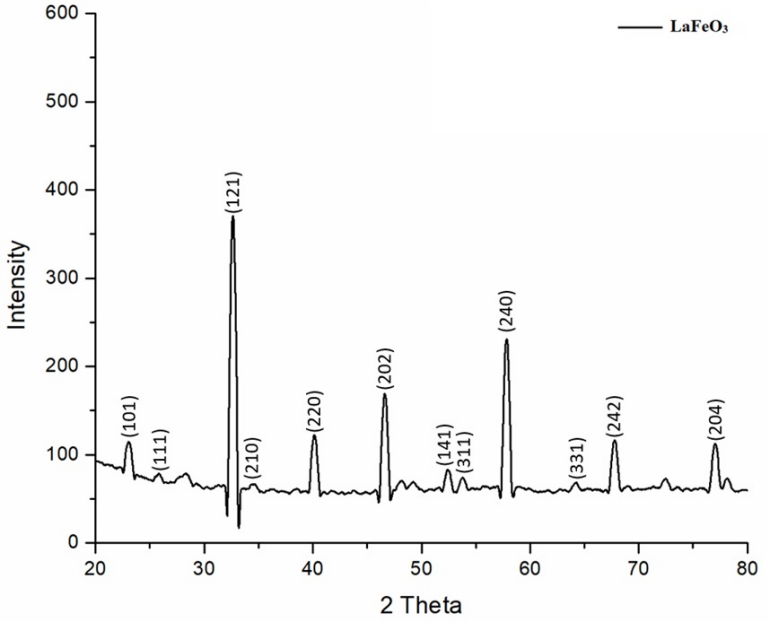

FIG. 7. XRD pattern of LFO-COP-1000 °C

temperature [42]. The average particle size is found 105, 130, 160 and 200 nm for the samples sintered at 1000 °C for 4, 8, 12 and 16 h, respectively. It depends on the diffusion rate of ions and the concentration of oxygen vacancies that cause the increase in grain boundries.

3.4. DC resistivity

The DC electrical resistance is measured by two-probe method. This method involves two electrical contacts, and each contact plays both roles of voltage measurement and current application [43]. The resistance can be determined by measuring the voltage drop across the sample when passing a constant known current across the samples. The results obtained from the resistance measurement are summarized in Fig. 10 and Table 2. As the heating time is increased, a slight decrease in resistance is observed. At the extended heating time, the excessive oxygen vacancies and the defects resulted in the low resistivity.

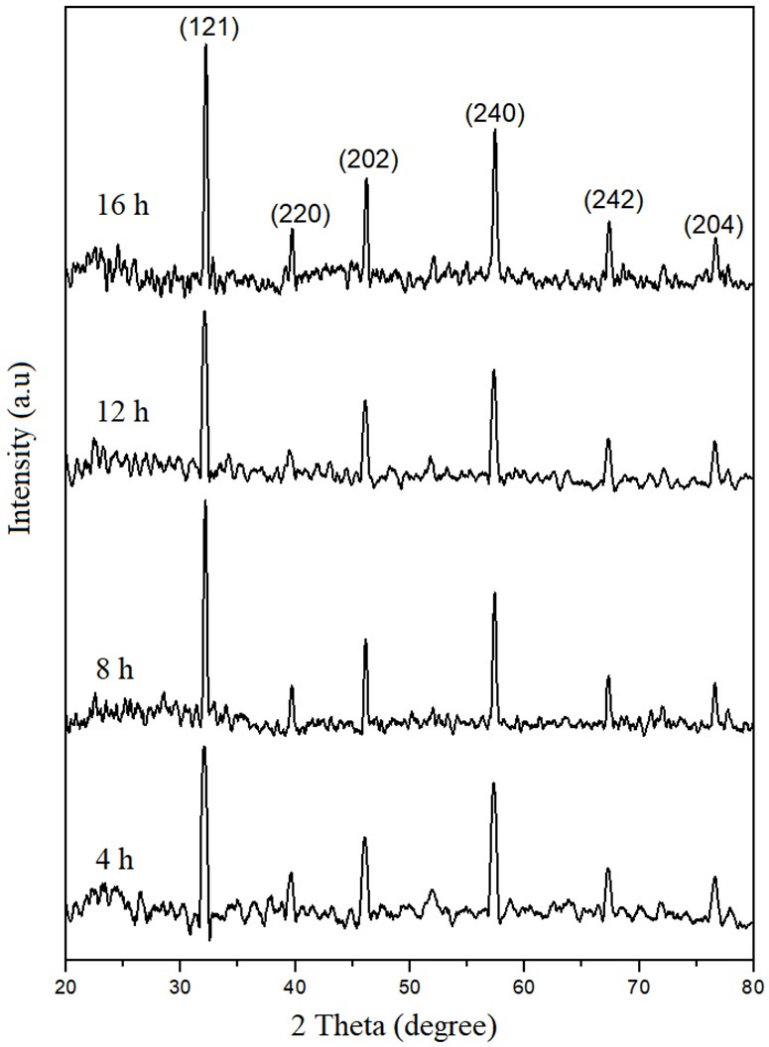

FIG. 8. XRD patterns of pellets sinterred at 1000 °C for different time

TABLE 2. The resistance of sintered sample at 1000 °C

Samples	Resistance (Ω)
LFO-COP-1000 °C 4 h	$16.1 \cdot 10^7$
LFO-COP-1000 °C 8 h	$15.4 \cdot 10^7$
LFO-COP-1000 °C 12 h	$12.6 \cdot 10^7$
LFO-COP-1000 °C 16 h	$10.7 \cdot 10^7$

3.5. Impedance spectroscopy

The impedance spectroscopy is applied to determine the electrical properties of $LaFeO_3$. At room temperature the frequency range 0 Hz to 10 MHz shows the frequency dependence of the dielectric constant (Fig. 11). The results exhibited that the high dielectric constant is due to grain-grain boundaries that changes with particle size, as the increase in heat treatment time resulted in higher grain size. The sample sintered at 1000 °C for 4 h displayed the lowest value at low frequency as compared to the sample at 16 h. This is the normal behavior of the dielectrics and the grain size distribution is narrow. Generally, four types of electric polarization processes (electronic, ionic, dipolar and space charge polarization) contribute to the dielectric properties [44]. At low frequency all of these polarizations are significant. At higher frequency space charge polarization gradually decreases. Therefore, the value of dielectric constant is constant at high frequency (10 MHz).

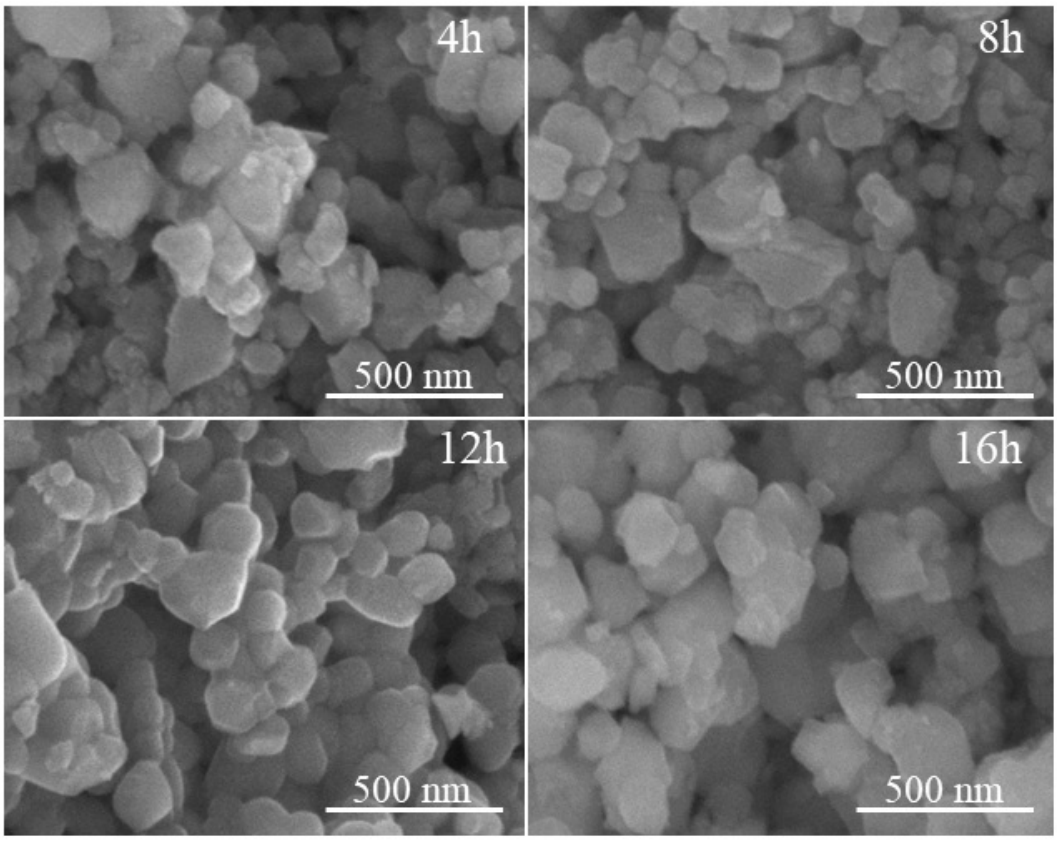

FIG. 9. SEM images of pellets sinterred at 1000 °C for different time

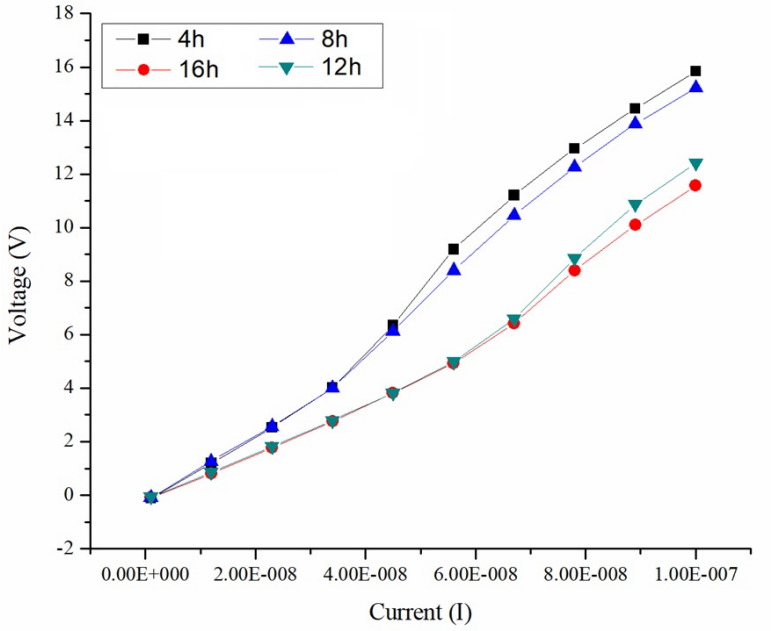

FIG. 10. The IV curve of the pellets sintered at1000 C for 4, 8, 12 and 16 h

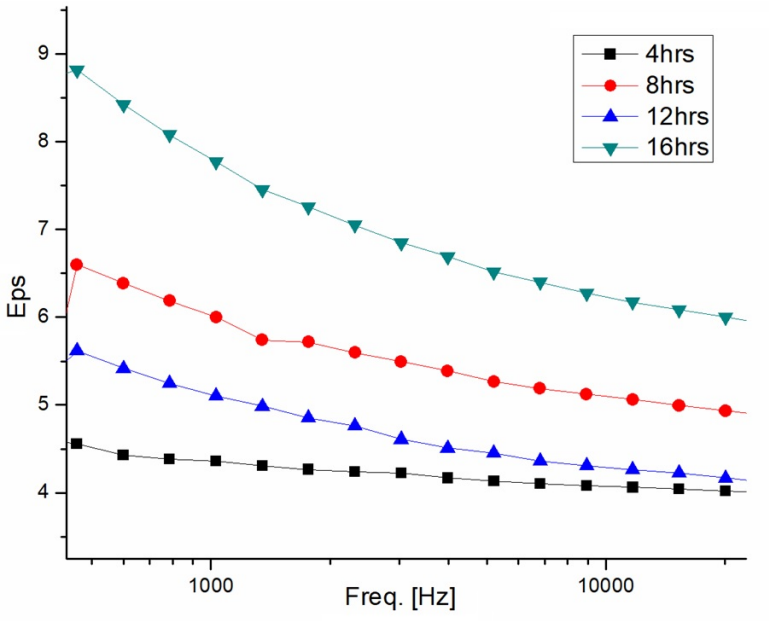

FIG. 11. The frequency dependance of dielectric constant

4. Conclusion

This study details the synthesis and characterization of perovskite-type $LaFeO_3$. The synthesized particles were characterized by XRD and the effect of sintering conditions on crystal symmetry and geometric structure is examined. It was found that an increase in temperature resulted in the transformation of amorphous hydroxide phases to the crystalline $LaFeO_3$ phase. It is also confirmed from XRD results that the synthesized perovskite-like $LaFeO_3$ has an orthorhombic unit cell with space group of pbnm. The unit cell parameters of $LaFeO_3$ were calculated as; $a = 5.563$, $b = 5.562$ and $c = 7.868$. The SEM results exhibited the semi-spherical particles with sharp grain boundaries. The particles were found in aggregation and expanded in size when sintered at high temperature. The average particle size of sintered pellets at 1000 °C for 4, 8, 12 and 16 h is determined 105, 130, 160 and 200 nm respectively. TGA analysis indicates that up to 800 °C of the hydroxides were strongly decomposed. However, after 800 °C weight loss is remarkably decreased. At 650 °C, 90% of the hydroxides were decomposed attributed to 27% weight loss. Two probe DC resistivity shows that resistance decreases with the increase in heat treatment and time due to excessive oxygen vacancies and an increase in particle size. Impedance spectroscopy displayed the high dielectric constant due to the grain-grain boundaries which change with particle size. Based on the results, perovskite-type $LaFeO_3$ material is proposed for practical application in energy and environmental fields.

References

[1] Shahid M.K., Batool A., Kashif A., Nawaz M.H., et al. Biofuels and biorefineries: Development, application and future perspectives emphasizing the environmental and economic aspects. *J. Environ. Manage.*, 2021, **297**, 113268.

[2] Khan S.A., Arshad Z., Shahid S., Arshad I., et al. Synthesis of TiO_2/Graphene oxide nanocomposites for their enhanced photocatalytic activity against methylene blue dye and ciprofloxacin. *Compos. Part B Eng.*, 2019, **175**, 107120.

[3] Wang H., Zheng H., Jiang Z., Dai Y., et al. Efficacies of biochar and biochar-based amendment on vegetable yield and nitrogen utilization in four consecutive planting seasons. *Sci. Total Environ.* 2017, **593–594**, P. 124–133.

[4] Shahid M.K., Kashif A., Fuwad A., Choi, Y. Current advances in treatment technologies for removal of emerging contaminants from water – A critical review. *Coord. Chem. Rev.*, 2021, **442**, 213993.

[5] Hasan S.A.U., Lee D.S., Im S.H., Hong K.H. Present Status and Research Prospects of Tin-based Perovskite Solar Cells. *Sol. RRL*, 2020, **4**, 1–30.

[6] Sri Gyan D., Dwivedi A., Roy P., Maiti T. Synthesis and thermoelectric properties of Ba_2TiFeO_6 double perovskite with insight into the crystal structure. *Ferroelectrics*, 2018, **536**, P. 146–155.

[7] Nguyen A.T., Phung V.D., Mittova V.O., Ngo H.D., et al. Fabricating nanostructured $HoFeO_3$ perovskite for lithium-ion battery anodes via co-precipitation. *Scr. Mater.*, 2022, **207**, 114259.

[8] Albadi Y., Martinson K.D., Shvidchenko A.V., Buryanenko I.V., et al. Synthesis of $GdFeO_3$ nanoparticles via low-temperature reverse co-precipitation: the effect of strong agglomeration on the magnetic behavior. *Nanosyst. Physics, Chem. Math.*, 2020, **11**, P. 252–259.

[9] Chang L., Li J., Le Z., Nie P., et al. Perovskite-type $CaMnO_3$ anode material for highly efficient and stable lithium ion storage. *J. Colloid Interface Sci.*, 2021, **584**, P. 698–705.

[10] Vo Q.M., Mittova V.O., Nguyen V.H., Mittova I.Y., et al. Strontium doping as a means of influencing the characteristics of neodymium orthoferrite nanocrystals synthesized by co-precipitation method. *J. Mater. Sci. Mater. Electron.*, 2021, **32**, P. 26944–26954.

[11] Tikhanova S.M., Lebedev L.A., Martinson K.D., Chebanenko M.I., et al. The synthesis of novel heterojunction h-$YbFeO_3$/o-$YbFeO_3$ photocatalyst with enhanced Fenton-like activity under visible-light. *New J. Chem.*, 2021, **45**, P. 1541–1550.

[12] Liu J., Sheha E., El-Dek S.I., Goonetilleke D., et al. $SmFeO_3$ and Bi-doped $SmFeO_3$ perovskites as an alternative class of electrodes in lithium-ion batteries. *CrystEngComm*, 2018, **20**, P. 6165–6172.
[13] Fossdal A., Menon M., Wiik K., Einarsrud M., et al. Crystal Structure and Thermal Expansion of $La_{1-x}Sr_xFeO_3$ materials. *J. Am. Ceram. Soc.*, 2004, **87**, P. 1952–1958.
[14] Scrimshire A., Lobera A., Bell A.M.T., Jones A.H., et al. Determination of Debye temperatures and Lamb-Mössbauer factors for $LnFeO_3$ orthoferrite perovskites (Ln = La, Nd, Sm, Eu, Gd). *J. Phys. Condens. Matter*, 2018, **30**, 105704.
[15] Seo J.W., Fullerton E.E., Nolting F., Scholl A., et al. Antiferromagnetic $LaFeO_3$ thin films and their effect on exchange bias. *J. Phys. Condens. Matter*, 2008, **20**, 264014.
[16] Wheeler G.P., Baltazar V.U., Smart T.J., Radmilovic A., et al. Combined Theoretical and Experimental Investigations of Atomic Doping to Enhance Photon Absorption and Carrier Transport of $LaFeO_3$ Photocathodes. *Chem. Mater.*, 2019, **31**, P. 5890–5899.
[17] Abdallah F.B., Benali A., Triki M., Dhahri E., et al. Effect of annealing temperature on structural, morphology and dielectric properties of $La_{0.75}Ba_{0.25}FeO_3$ perovskite. *Superlattices Microstruct.*, 2018, **117**, P. 260–270.
[18] Gosavi P.V., Biniwale R.B. Pure phase $LaFeO_3$ perovskite with improved surface area synthesized using different routes and its characterization. *Mater. Chem. Phys.*, 2010, **119**, P. 324–329.
[19] Nakayama S., $LaFeO_3$ perovskite-type oxide prepared by oxide-mixing, co-precipitation and complex synthesis methods. *J. Mater. Sci.*, 2001, **36**, P. 5643–5648.
[20] Sivakumar M., Gedanken A., Zhong W., Jiang Y.H., et al. Sonochemical synthesis of nanocrystalline $LaFeO_3$. *J. Mater. Chem.*, 2004, **14**, P. 764–769.
[21] Qi X., Zhou J., Yue Z., Gui Z., et al. A simple way to prepare nanosized $LaFeO_3$ powders at room temperature. *Ceram. Int.*, 2003, **29**, P. 347–349.
[22] Yang Z., Huang Y., Dong B., Li H.L. Controlled synthesis of highly ordered $LaFeO_3$ nanowires using a citrate-based sol-gel route. *Mater. Res. Bull.*, 2006, **41**, P. 274–281.
[23] Wang Y., Zhu J., Zhang L., Yang X., et al. Preparation and characterization of perovskite $LaFeO_3$ nanocrystals. *Mater. Lett.*, 2006, **60**, P. 1767–1770.
[24] Su H., Jing L., Shi K., Yao C., et al. Synthesis of large surface area $LaFeO_3$ nanoparticles by SBA-16 template method as high active visible photocatalysts. *J. Nanoparticle Res.*, 2010, **12**, P. 967–974.
[25] Tang P., Tong Y., Chen H., Cao F., et al. Microwave-assisted synthesis of nanoparticulate perovskite $LaFeO_3$ as a high active visible-light photocatalyst. *Curr. Appl. Phys.*, 2013, **13**, P. 340–343.
[26] Liu T., Xu Y. Synthesis of nanocrystalline LaFeO3 powders via glucose sol-gel route. *Mater. Chem. Phys.*, 2011, **129**, P. 1047–1050.
[27] Idrees M., Nadeem M., Atif M., Siddique M., et al. Origin of colossal dielectric response in $LaFeO_3$. *Acta Mater.*, 2011, **59**, P. 1338–1345.
[28] Köferstein R., Jäger L., Ebbinghaus, S.G., Magnetic and optical investigations on $LaFeO_3$ powders with different particle sizes and corresponding ceramics. *Solid State Ionics*, 2013, **249**–**250**, 1–5.
[29] Thuy N.T., Minh D. Le, Size effect on the structural and magnetic properties of nanosized perovskite $LaFeO_3$ prepared by different methods. *Adv. Mater. Sci. Eng.*, 2012, 380306.
[30] Liu W., Zeng X., Liu S., Zhu Y., et al. Growth and characterization of $LaFeO_3$ crystals. *Key Eng. Mater.*, 2014, **602**–**603**, P. 27–31.
[31] Idrees M., Nadeem M., Siddiqi S.A., Ahmad R., et al. The organic residue and synthesis of $LaFeO_3$ by combustion of citrate and nitrate precursors. *Mater. Chem. Phys.*, 2015, **162**, P. 652–658.
[32] Vijayaraghavan T., Bradha M., Babu P., Parida K.M., et al. Influence of secondary oxide phases in enhancing the photocatalytic properties of alkaline earth elements doped $LaFeO_3$ nanocomposites. *J. Phys. Chem. Solids*, 2020, **140**, 109377.
[33] Zhao F., Bai Z., Fu Y., Zhao D., et al. Tribological properties of serpentine, $La(OH)_3$ and their composite particles as lubricant additives. *Wear*, 2012, **288**, P. 72–77.
[34] Kang J.G., Kim Y. Il, Won Cho D., Sohn Y. Synthesis and physicochemical properties of $La(OH)_3$ and La_2O_3 nanostructures. *Mater. Sci. Semicond. Process.*, 2015, **40**, P. 737–743.
[35] Lazarević Z.Ž., Jovalekić Č., Recnik A., Ivanovski V.N., et al. Study of manganese ferrite powders prepared by a soft mechanochemical route. *J. Alloys Compd.*, 2011, **509**, P. 9977–9985.
[36] Shahid M.K., Choi Y. Characterization and application of magnetite Particles, synthesized by reverse coprecipitation method in open air from mill scale. *J. Magn. Magn. Mater.*, 2020, **495**, 165823.
[37] Kabir H., Nandyala S.H., Rahman M.M., Kabir M.A., et al. Influence of calcination on the sol–gel synthesis of lanthanum oxide nanoparticles. *Appl. Phys. A Mater. Sci. Process.*, 2018, **124**, 1–11.
[38] Boumaza S., Boudjellal L., Brahimi R., Belhadi A., et al. Synthesis by citrates sol-gel method and characterization of the perovskite $LaFeO_3$: application to oxygen photo-production. *J. Sol-Gel Sci. Technol.*, 2020, **94**, P. 486–492.
[39] Al-Mamari R.T., Widatallah H.M., Elzain M.E., Gismelseed A.M., et al. Structural, Mössbauer, and Optical studies of mechano-synthesized Ru^{3+}-doped $LaFeO_3$ nanoparticles. *Hyperfine Interact.*, 2021, **243**, 4.
[40] Thirumalairajan S., Girija K., Ganesh I., Mangalaraj D., et al. Controlled synthesis of perovskite $LaFeO_3$ microsphere composed of nanoparticles via self-assembly process and their associated photocatalytic activity. *Chem. Eng. J.*, 2012, **209**, P. 420–428.
[41] Thirumalairajan S., Girija K., Mastelaro V.R., Ponpandian N. Photocatalytic degradation of organic dyes under visible light irradiation by floral-like $LaFeO_3$ nanostructures comprised of nanosheet petals. *New J. Chem.*, 2014, **38**, P. 5480–5490.
[42] Tho N.D., Huong D., Van Ngan P.Q., Thai G.H., et al. Effect of sintering temperature of mixed potential sensor Pt/YSZ/$LaFeO_3$ on gas sensing performance. *Sensors Actuators B Chem.*, 2016, **224**, P. 747–754.
[43] Wang S., Wang D., Chung D.D.L., Chung J.H. Method of sensing impact damage in carbon fiber polymer-matrix composite by electrical resistance measurement. *J. Mater. Sci.*, 2006, **41**, P. 2281–2289.
[44] Pirzada B.M., Sabir S. Polymer-based nanocomposites for significantly enhanced dielectric properties and energy storage capability, in: *Polymer-Based Nanocomposites for Energy and Environmental Applications*, Elsevier Ltd., 2018, P. 132–183.

Submitted 2 November 2021; revised 20 April 2022; accepted 22 April 2022

Information about the authors:

Muhammad Irfan Asghar – Department of Physics, COMSATS University Islamabad, Lahore Campus, Pakistan; irfanmeo1@gmail.com

Muhammad Kashif Shahid – Research Institute of Environment & Biosystem, Chungnam National University, Daejeon, Republic of Korea; mkbutt2000@gmail.com

Muhammad Haq Nawaz – Department of Physics, University of Gujrat, Hafiz Hayat Campus, Gujrat, Pakistan; haqn5656@gmail.com

Muhammad Idrees – Department of Physics, COMSATS University Islamabad, Lahore Campus, Pakistan; midrees@cuilahore.edu.pk

Muhammad Asif – Department of Physics, University of Engineering and Technology Lahore, Pakistan; asif81292@yahoo.com

Ahsan Ali – School of Mechanical Engineering, University of Leeds, Leeds LS2 9JT, UK; ahsanali23654@gmail.com

Conflict of interest: the authors declare no conflict of interest.